Posture-specific phantoms representing female and male adults in Monte Carlo-based simulations for radiological protection

V F Cassola, R Kramer, C A B de Oliveira Lira and H J Khoury

Department of Nuclear Energy, Federal University of Pernambuco, Avenida Prof. Luiz Freire, 1000, CEP 50740-540, Recife, Brazil

E-mail: rkramer@uol.com.br

Statement of provenance:
'This is an author-created, un-copyedited version of an article accepted for publication in Physics in Medicine and Biology. IOP Publishing Ltd is not responsible for any errors or omissions in this version of the manuscript or any version derived from it. The definitive publisher authenticated version is available at doi:10.1088/0031-9155/55/15/014.'

Abstract

Has the posture of a patient an effect on the organ and tissue absorbed doses caused by X-ray examinations? This study wants to find the answer to this question, based on Monte Carlo (MC) simulations of commonly performed X-ray examinations using adult phantoms modelled to represent humans in standing as well as in supine posture. The recently published FASH (Female Adult meSH) and MASH (Male Adult meSH) phantoms have standing posture. In a first step, both phantoms were updated with respect to their anatomy: Glandular tissue was separated from adipose tissue in the breasts, visceral fat was separated from subcutaneous fat, cartilage was segmented in ears, nose and around the thyroid, the right lung is now 15% greater than the left lung. The updated versions are called FASH2_sta and MASH2_sta (sta = standing). Taking into account the gravitational effects on organ position and fat distribution, supine versions of the FASH2 and the MASH2 phantoms have been developed in this study and called FASH2_sup and MASH2_sup. MC simulations of external whole body exposure to monoenergetic photons and partial body exposure to X-rays have been made with the standing and supine FASH2 and MASH2 phantoms. For external whole body exposure for AP and PA projection with photon energies above 30 keV, the effective dose did not change by more than 5% when the posture changed from standing to supine or vice versa. Apart from that, supine posture is quite rare in occupational radiation protection from whole body exposure. However, in X-ray diagnosis supine posture is frequently used for patients submitted to examinations. Changes of organ absorbed doses up to 60% were found for simulations of chest and abdomen radiographs if the posture changed from standing to supine or vice versa. Further increase of differences between posture-specific organ and tissue absorbed doses with increasing whole body mass is to be expected.

1. Introduction

Depending on the X-ray procedure to undergo, patients have to take up specific postures when being positioned between X-ray tube and imaging system. Standing or lying, each posture affects the position of internal organs and the distribution of adipose tissue due to the influence of the gravitational force. Consequently, exposed parts of the body may have different diameters in the direction of the radiation and organs may have been shifted relative to the X-ray field. Such anatomical changes can have a significant effect on organ and tissue absorbed doses and associated radiation risks for patients submitted to examinations in X-ray diagnosis.

In the past, most studies on organ absorbed dose assessment in X-ray diagnosis were made using computational human phantoms, some of which, called stylized phantoms, were representing standing patients (Kramer and Drexler 1976, Rosenstein 1976, Jones and Wall 1985, Rosenstein 1988, Drexler et al 1990, Le Heron 1992, Hart et al 1994, Schultz et al 1994, Schultz et al 1995, Petoussi-Henss et al 1995), while others, mainly voxel or hybrid phantoms, were representing patients lying on the back (Zankl et al 2000, Akahane et al 2001, Winslow et al 2004, Petoussi-Henss et al 2005, Bozkurt and Bor 2007, Kramer et al 2008, Johnson et al 2009). More recently, a mesh-based standing phantom was used for absorbed dose comparison with a standing stylized phantom for CT examinations (Liu et al 2010).

In order to investigate the effect of posture and position of the patient on organ and tissue absorbed doses in X-ray diagnosis, one would have to use phantoms modelled to represent different postures. For whole body exposure, such an approach was reported by Sato et al (2007, 2008a, b), who developed two different voxel phantoms based on whole body CT images of a Japanese volunteer scanned in lying as well as in standing posture. Their results for organ positions showed cranial shifts for the adrenals, kidneys, liver, pancreas, small intestine, and urinary bladder between 0.3 and 1.9 cm, and an increase of the waist circumference, when the posture changed from standing to lying. As for dosimetry, up to 14% "posture effect" was found between organ absorbed doses for internal photon emitters, while conversion coefficients for external monoenergetic photon exposure showed greater differences. For whole body irradiation anterior-posterior (AP) and posterior-anterior (PA), Sato et al determined ratios between organ absorbed doses for lying and for standing posture. The ratios showed a minimum of 0.42 and maximum of 4.0 for incident photon energies below 50 keV, which is exactly the range for mean photon energies of many X-ray spectra. Due to partial body exposure, additional differences can be expected in X-ray diagnosis, where organ absorbed doses dependent crucially on the position of the organ relative to the boundaries of the X-ray field.

Recently, numerous studies on the absorption of electromagnetic fields (EMF) by the human body have investigated the effect of the posture (Findlay and Dimbylow 2005, Nagaoka and Watanabe 2008, Dimbylow and Findlay 2010, Uustitupa et al 2010). Changing the positions of arms and legs relative to the head and the trunk of the body were primary concern of these investigations, and efforts were made to keep internal organs at fixed positions. Therefore, anatomical data relevant for the current study could not be found in the quoted EMF publications.

FASH and MASH are adult female and male human phantoms, respectively, recently developed based on polygon mesh surfaces (Cassola et al 2010). FASH is the acronym for *F*emale *A*dult me*SH*, MASH means *M*ale *A*dult me*SH*, and both phantoms represent humans in standing posture. In this study, updated versions of the standing phantoms, called FASH2 and MASH2, were developed and then lying versions of the FASH2 and the MASH2 phantoms were designed in order to investigate the dosimetric consequences of posture variations for patients submitted to X-ray radiography. First, the methods will be explained, which were used to update the standing phantoms, then to transform the standing phantoms into lying phantoms, and finally to carry out radiographic simulations applying Monte Carlo techniques using the EGSnrc Monte Carlo code (Kawrakow 2000a, b, Kawrakow and Rogers 2003). Second, the results will show the anatomy of the phantoms and dosimetric data for external whole body exposure and for examinations of the chest and the abdomen to demonstrate the effect of the body posture on organ and tissue absorbed doses.

2. Materials and methods

2.1 Posture and position

Some medical terms used in radiology need to be addressed in order to understand the terminology applied to the characterization of the exposure conditions and the interpretation of results presented in this study. In X-ray diagnosis, the most frequent postures used for imaging of patients are standing (orthostatic) and lying (decubitus or recumbent).

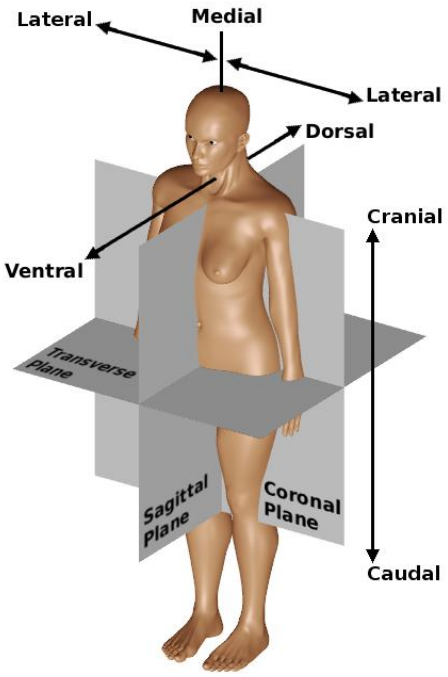

Figure 1. Medical terms used in radiology to describe the position of the patient.

Figure 1 describes the positions a human body can have relative to the X-ray beam for any of these postures. For example, dorsal means that the radiation is directed towards the frontal part of the body to reach the image receptor located behind the patient. A dorsal position is used for radiographs made in standing or lying posture and is also called an AP projection. If the X-rays enter the patient's body at the back to reach the image receptor in front of the patient, the position is called ventral, which represents a PA projection. Radiological terms are also used to describe movements of organs, in cranial or caudal direction, for example. Images representing cuts through the patient's body are classified as transverse, coronal or sagittal. Standard CT images represent transverse cuts through the body, for example.

For standing posture, different body positions do not cause significant anatomical changes, because the direction of the gravitational force relative to the body is always the same, namely caudal. For lying posture, organ locations and fat distribution change with every new position of the body. To model phantoms for each possible position of the lying posture is beyond the scope of this study. Apart from phantoms suitable for most positions of the standing posture, this paper also presents male and female adult phantoms for supine (lying/dorsal) posture, thereby covering the most important combinations of posture and position used in X-ray diagnosis. Phantoms for prone (lying/ventral) posture will be discussed but not developed in this study.

2.2 The standing FASH2/MASH2 phantoms

The *F*emale *A*dult me*SH* (FASH) and the *M*ale *A*dult me*SH* (MASH) phantoms (Cassola et al 2010) have been developed based on polygon mesh surfaces using the open source software tools MakeHuman (MakeHuman 2009), Blender (Blender 2009), Binvox (Min 2009, Nooruddin and Turk 2003) and ImageJ (ImageJ 2009). Representing standing adults, FASH and MASH have organ and tissue masses, body height and mass adjusted to the reference data given by ICRP89 (ICRP 2002). Figure 2 presents frontal views of the FASH and MASH mesh phantoms, showing transparent surfaces with skeletons, organs and tissues underneath, while figure 3 shows the skin of the voxelized versions. The FASH and the MASH phantoms have been used for Monte Carlo simulation of whole

body exposure to ionizing radiation and the results have been compared with corresponding data from other phantoms (Kramer et al 2010).

FASH MASH

Figure 2. FASH (left) and MASH (right) mesh phantoms: organs, skeleton, muscle, adipose and transparent skin

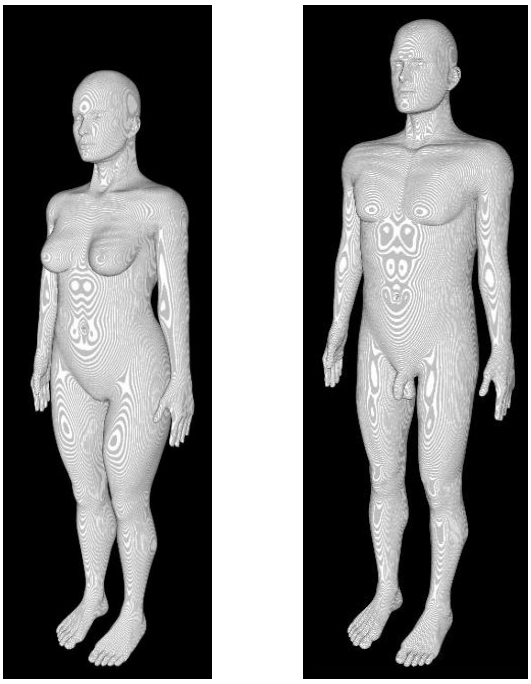

FASH MASH

Figure 3. FASH (left) and MASH (right) voxel phantoms: surfaces

The development of phantoms for supine posture was used as an opportunity to revise and updated some of the organs and tissues of the FASH and the MASH phantoms. The mass of the right lung is now 15% greater than the left lung based on information taken from ICRP89 (2002). The breasts have been segmented into glandular and adipose tissue in both phantoms using information from ICRP89 (ICRP 2002) and from ICRP95 (ICRP 2004). Trachea and bronchi were segmented as walled organs filled with air. Subcutaneous and visceral fat (adipose) were separated. Cartilage was segmented also in the ears, the nose and around the thyroid. The changes and additions are significant and therefore the new names FASH2 and MASH2. In the voxelized FASH2 and MASH2 phantoms, the cubic voxel size of 1.2 mm x 1.2 mm x 1.2 mm was maintained.

2.3 The supine FASH2/MASH2 phantoms

When a standing person takes up a supine posture, the gravitational force causes the following anatomical effects:

- Cranial and/or dorsal shifts of organs
- Compression of the lung volume in cranial and dorsal directions caused by the heart and abdominal organs
- Reduction of sagittal diameters, especially the abdominal, and an increase of lateral diameters, especially at the dorsal part of the lower abdomen
- Change of position of shoulders, arms and associated bones in dorsal direction

2.3.1 Shift of organs

Sato et al (2007, 2008a, b) found dislocations of centres of mass for several abdominal organs in cranial direction between 0.3 and 1.9 cm, when the posture of a Japanese adult male changed from standing to supine. Concerned about the correct block placement for the kidneys during total body irradiation, Reiff et al (1999) investigated the changes in size and location of the kidneys in 15 Caucasian patients. They found an average cranial shift of 3.6 cm for the kidneys when the patient's posture changed from standing to supine. Taking into account on the one hand the comprehensive set of data for one subject published by Sato et al, and on the other hand Reiff et al's larger sample size (15 vs. 1) and also the ethnic differences between Asians and Caucasians, the organ shifts applied to the Caucasian FASH2 and MASH2 phantoms were those given by Sato et al but corrected with the ratio of the kidney shifts: 3.6 cm (Reiff) / 1.9 cm (Sato) = 1.9. Table 1 shows the organ-specific cranial shifts given by Sato et al (2007, 2008a, b), the calculated data based on the correction factor of 1.9 and the cranial organ shifts actually realized in the MASH2 and FASH2 phantoms. The realized shifts deviate sometimes from the calculated data because organ overlaps had to be avoided. Some organs, for which dislocation data were not available, had to be moved as well. Their cranial shifts, also shown in table 1, are the result of avoiding overlaps with neighbouring organs. In the publications of Sato et al (2007, 2008a, b), dorsal organ shifts were not given. Dorsal shifts, shown in table 1, were derived from data on ventral organ shifts found in the paper by Ball et al (1980), also mentioned further down in section 2.4. Here, the term "shift" is used for a dislocation of the centre of mass of an organ relative to the pelvis, a bone assumed not to change its position when the posture changes from standing to supine.

2.3.2 Compression of the lung volume

Almost all investigations concerned with the effect of posture on pulmonary functions were made with patients, i.e. subjects with a pulmonary or other health condition, and were studying the change from sitting posture to either the supine or the prone posture. Blair and Hickam (1955), however, investigated the effect of posture on the lung volume in normal subjects and included also the standing posture in their study. For 9 subjects they found for the total capacity of the lungs mean

Table 1. Cranial and dorsal shifts of the centres of mass of organs in the MASH2 and in the FASH2 phantoms when the posture changes from standing to supine

Shift of the center of mass Sta >>>> Sup	Sato et al cranial (cm)	calculated cranial (cm)	MASH2 cranial (cm)	MASH2 dorsal (cm)	FASH2 cranial (cm)	FASH2 dorsal (cm)
Adrenals	1.0	1.9	2.0	0.8	1.8	0.0
Kidneys	1.9	3.6	3.3	1.2	3.6	0.5
Liver	1.0	1.9	1.7	0.7	1.6	0.1
Stomach	1.4	2.7	2.6	0.5	2.7	0.4
Pancreas	1.0	1.9	1.9	0.3	1.9	0.5
Urinary bladder	0.4	0.8	0.9	0.2	0.9	0.2
Colon	0.3	0.6	0.5	0.3	0.5	1.4
Small intestine	1.2	2.3	2.5	0.4	2.0	0.9
Heart			2.0	0.1	1.9	0.0
Lungs			1.4	0.5	1.1	0.3
Thymus			2.0	0.1	2.0	0.3
Spleen			1.8	0.5	1.4	0.1
Uterus					0.9	1.2
Ovaries					1.1	1.1

values of 6.77 L and 6.22 L for the standing and supine posture, respectively. This decrease, caused by pressure from the heart and abdominal organs, was used to reduce the lower dorsal part of the lung volume in the supine FASH2 and MASH2 phantoms by 8%. Then, the position of the diaphragm was re-adjusted in order to remain in contact with the lungs. The heart and abdominal organs were moved into the space liberated by the lungs, observing the organ-specific cranial and dorsal shifts given in table 1.

2.3.3 Reduction of the sagittal abdominal diameter (SAD)

In a study on "Pulmonary Function and Abdominal Adiposity in the General Public" based on 2153 subjects, Ochs-Balcom et al (2006) determined a variety of anthropometric parameters, among them the abdominal height "defined as the sagittal diameter of the abdomen measured by interviewers at the iliac crest while the participant was in the supine position". For the 50th SAD percentiles the authors found 20.8 cm and 18.7 cm for the male and the female adult, respectively. Investigating the relationship between SAD and coronary heart disease risk among more than 45000 participants, Iribarren et al (2006) determined the SADs for standing posture "midway between the lower rib margin and the superior anterior iliac crest", i.e. at the height of the waist circumference. This study reports 21.0 cm and 19.0 cm for the 50th percentile of the male and the female adult SAD, respectively. Unfortunately, the SADs of the two studies cannot be compared because they refer to different measurement locations. In order to link the data from Iribarren et al (2006) to the iliac position, ratios between SADs measured at the iliac crest and at the waist circumference were determined in the standing MASH2 and FASH2 phantoms. For the male adult this ratio was found to be 1.05, for the female adult 1.07. Consequently, the SADs of the standing MASH2 and FASH2 phantoms were reduced by a factor of 20.8 cm / (21.0 cm x 1.05) = 0.94 or by 6%, and of 18.7 cm / (19.0 cm x 1.07) = 0.92 or by 8%, respectively, to receive the SADs at the iliac crest for the supine phantoms, while keeping the circumference constant at the same time. This led to a slight increase of the lateral diameter, of course. Adjustment of the position of shoulders and arms for supine posture were made based on trials with volunteers. These adjustments affect also some bones in the thorax. In the thoracic region, the supine spine has less curvature compared to the standing spine (Sato et al 2007a, b, 2008). Because of the bones, reduction of the sagittal diameter in the thorax region is less than for the abdomen. The adjustments of the bone positions did not change the volumes of the segmented skeletal tissues.

2.4 The prone body position

Using CT imaging in computer-assisted treatment planning for patients treated at the Los Alamos Pi-Meson Facility, Ball et al (1980) studied the positional variation of anatomic structures in 38 patients for supine and prone body position prior to radiotherapy. Turning the patients from supine to prone position caused movements of the liver, pancreas, spleen, heart, great vessels, kidneys, stomach and colon up to 2 cm ventrally and up to 6 cm caudally. Consequently, pressure by these organs on the lungs decreased significantly and, additionally, Albert and Hubmayr (2000) found that compared to the supine position, "The prone position eliminates compression of the lungs by the heart". Thus, with respect to lung volume and organ positions, the prone posture is more similar to the standing posture, while at the same time being more similar to the supine posture with regard to the fat distribution. Technically there is no problem with developing phantoms in prone posture as well, however, it was found that in text books for X-ray technicians only very few examinations are using the prone posture (Becht et al 2008, Bontrager 2003) and, in addition, it turned out that prone X-ray procedures are very rarely performed in radiological practice (Bein 2010, Bauer 2010). Therefore, phantoms for prone body position were not developed in this study. However, at least the data from Ball et al (1980) were helpful for the assessment of the dorsal shifts shown in table 1.

2.5 Monte Carlo simulations

Organ and tissue absorbed dose calculations for external whole body and radiographic exposure to photons have been made with the EGSnrc Monte Carlo code connected to the MASH2_sta, MASH2_sup, FASH2_sta, FASH2_sup phantoms (sta = standing, sup = supine). The method used is the same described in Kramer et al (2010), i.e. deposition of radial energy in organs and tissues was calculated based on coupled transport of photons and electrons in all segmented organs and tissues, and by additionally using μCT images of human spongiosa for the determination of absorbed dose to radiosensitive skeletal tissues. Absorbed doses to organs and tissues were normalized to air kerma free in air, which was calculated simultaneously based on the air kerma-to-fluence conversion function for photons (ICRP 1996) during radiation transport through the phantoms, i.e. that the results were determined as conversion coefficients. Based on the proportionality between absorbed dose and energy deposited, a statistical error in percent was calculated for each organ and tissue absorbed dose as $100 \times \sigma / E_{av}$, where σ represents the standard deviation for the energy deposited in an organ or tissue and E_{av} the mean energy deposited per incident photon. Outside the skeleton, the smallest segmented organs or tissues still have ca. 5800 voxels, i.e. that because of the 1.2 mm cubic voxel size, voxel effects caused by segmentation procedures have negligible effect on the absorbed dose averaged over the organ or tissue volume, and even more so for larger organs and tissues. In the microstructure of trabecular bone, based on 60 μm cubic voxels, voxel effects may influence the absorbed dose to the bone surface cells by up to 5% which was discussed earlier (Kramer et al 2006).

The number of the tissues used in this study was updated. Apart from the 9 tissue compositions used before (Kramer et al 2010), which were taken from ICRU46 (ICRU 1992), additional 13 tissue compositions, partly sex-specific, have been compiled based on data found in Publication 110 on the ICRP reference phantoms (ICRP 2009), which uses 53 different tissue compositions. Table 2 shows the compositions for the 9 tissues taken from ICRU46 and additionally for the teeth, blood and lymphatic tissue taken from ICRP110 and applied to the phantoms for both sexes. In table 3 on the left, SOFT F103, SOFT F104 and SOFT F105 represent compositions averaged over several female-specific soft tissue compositions from ICRP110 with densities of 1.03, 1.04 and 1.05 g/cm^3, respectively, while FEYES and FGLAND stand for the female-specific compositions of the eyes and the glandular tissue, respectively. The corresponding male-specific compositions are given in table 3 on the right.

Table 2. Tissue compositions from ICRU46 (ICRU1992) and ICRP110 (ICRP 2009) for adults of both sexes

Element	Muscle Tissue [%]	Adipose Tissue [%]	Skin Tissue [%]	Lungs Tissue [%]	Skeleton Cartilage [%]	Skeleton Bone [%]	Skeleton Spongiosa [%]	Skeleton YBM [%]	Skeleton RBM [%]	Skeleton Teeth [%]	Blood Tissue [%]	Lymphatic Tissue [%]
H	10.2	11.4	10.0	10.3	9.6	3.4	8.5	11.5	10.5	2.2	10.2	10.8
C	14.3	59.8	20.4	10.5	9.9	15.5	40.4	64.4	41.4	9.5	11.0	4.2
N	3.4	0.7	4.2	3.1	2.2	4.2	2.8	0.7	3.4	2.9	3.3	1.1
O	71.0	27.8	64.5	74.9	74.4	43.5	36.7	23.1	43.9	42.1	74.5	83.1
Na	0.1	0.1	0.2	0.2	0.5	0.1	0.1	0.1			0.1	0.3
Mg						0.2	0.1			0.7		
P	0.2		0.1	0.2	2.2	10.3	3.4		0.1	13.7	0.1	
S	0.3	0.1	0.2	0.3	0.9	0.3	0.2	0.1	0.2		0.2	0.1
Cl	0.1	0.1	0.3	0.3	0.3		0.2	0.1	0.2		0.3	0.4
K	0.4		0.1	0.2			0.1		0.2		0.2	
Ca						22.5	7.4			28.9		
Fe							0.1		0.1		0.1	
ρ [gcm^{-3}]	1.05	0.95	1.09	0.26	1.1	1.92	1.18	0.98	1.03	2.75	1.06	1.03

Table 3. Soft tissue compositions based on ICRP110 (ICRP 2009) for adult females (F) and males (M)

Element	SOFT F103 Tissue [%]	SOFT F104 Tissue [%]	SOFT F105 Tissue [%]	FEYES Tissue [%]	FGLAND Tissue [%]	SOFT M103 Tissue [%]	SOFT M104 Tissue [%]	SOFT M105 Tissue [%]	MEYES Tissue [%]	MGLAND Tissue [%]
H	10.5	10.5	10.4	9.7	11.4	10.4	10.5	10.4	9.7	11.2
C	24.3	10.9	13.9	18.3	46.1	22.4	10.9	13.8	18.1	51.6
N	2.7	2.6	2.7	5.4	0.5	2.8	2.6	2.8	5.3	1.1
O	61.6	75.2	71.8	66.0	42.0	63.4	75.2	71.9	66.3	35.8
Na	0.1	0.1	0.2	0.1		0.1	0.1	0.2	0.1	0.1
Mg										
P	0.2	0.1	0.2	0.1		0.2	0.1	0.2	0.1	
S	0.3	0.1	0.2	0.3		0.3	0.1	0.2	0.3	0.1
Cl	0.2	0.2	0.2	0.1		0.2	0.2	0.2	0.1	0.1
K	0.2	0.2	0.3			0.2	0.2	0.3		
Ca										
Fe										
ρ [gcm^{-3}]	1.03	1.04	1.05	1.05	1.02	1.03	1.04	1.05	1.05	1.02

3. Results

3.1 The standing FASH2/MASH2 phantoms

The development of the FASH and the MASH phantoms has extensively been described in the paper of Cassola et al (2010). Therefore, this section presents only properties of some organs and tissues updated in the FASH2_sta and the MASH2_sta phantoms. Among the newly segmented tissues are adipose and glandular tissue in the breasts, shown in figure 4 for the female phantom, and visceral fat separated from subcutaneous fat, shown in figure 5 for the male phantom.

Figure 4. Glandular tissue and adipose segmented in the FASH2_sta phantom

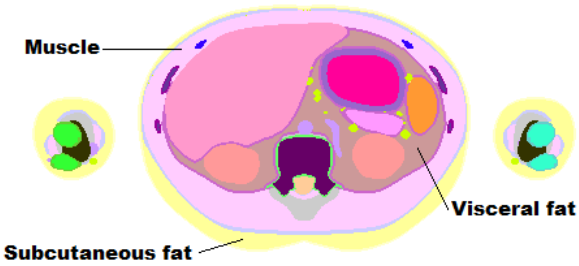

Figure 5. Subcutaneous and visceral fat (adipose) segmented in the MASH2_sta phantom

Glandular tissue is the tissue relevant with respect to radiation risk for the breasts (Feig 1980, Rubin and Strayer 2008) and anatomically correct segmentation is therefore warranted. The separation of subcutaneous and visceral fat can be helpful for the modelling of obese phantoms, because mass increase by fat does not necessarily occur uniformly throughout all fatty regions of the human body. For reference, segmented skeletal tissue volumes as well as all organ and tissue masses of the FASH2 and the MASH2 phantoms are given in the appendix.

3.2 The supine FASH2 and MASH2 phantoms

Using the Blender software, the phantoms FASH2_sta and MASH2_sta have been changed based on the data and criteria for female and male supine adults described in section 2.3. The surfaces of the mesh phantoms FASH2_sup and MASH2_sup, representing adults of supine posture, are presented in figures 6 – 9 for frontal and lateral views together with the standing phantoms FASH2_sta and MASH2_sta for comparison.

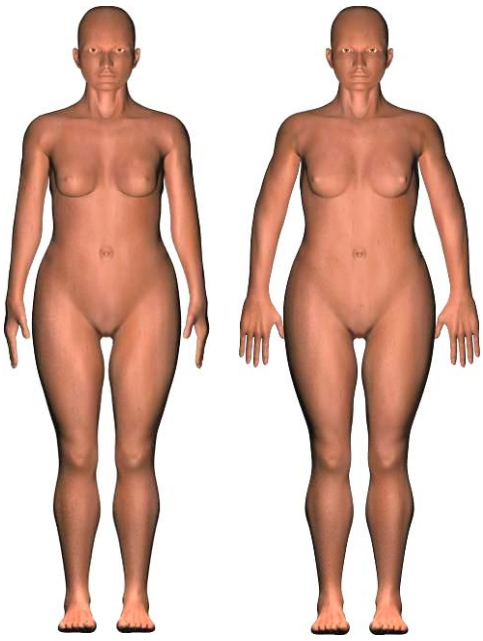

Figure 6. FASH2_sta and FASH2_sup: frontal view of surfaces

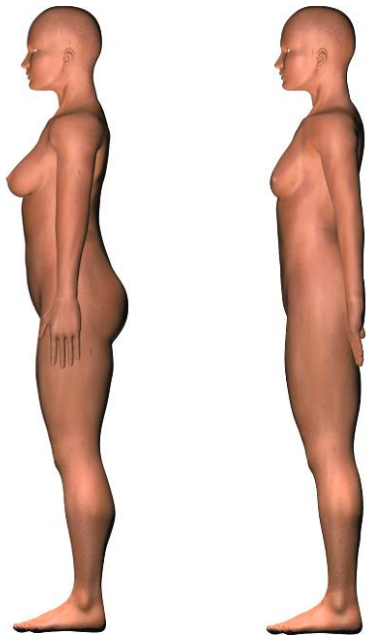

Figure 7. FASH2_sta and FASH2_sup: lateral view of surfaces

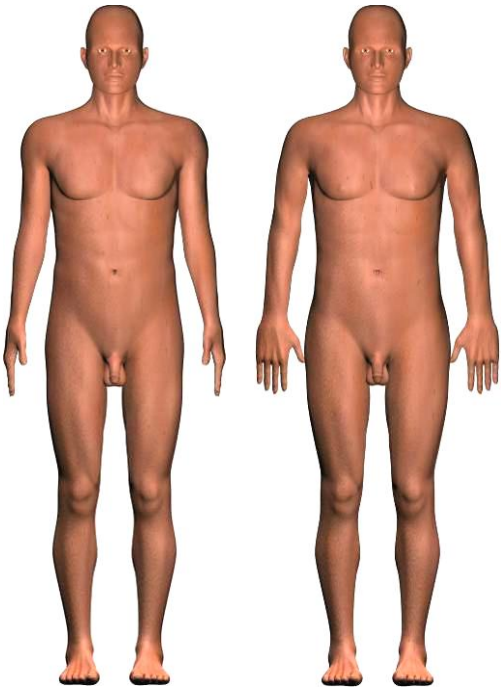

Figure 8. MASH2_sta and MASH2_sup: frontal view of surfaces

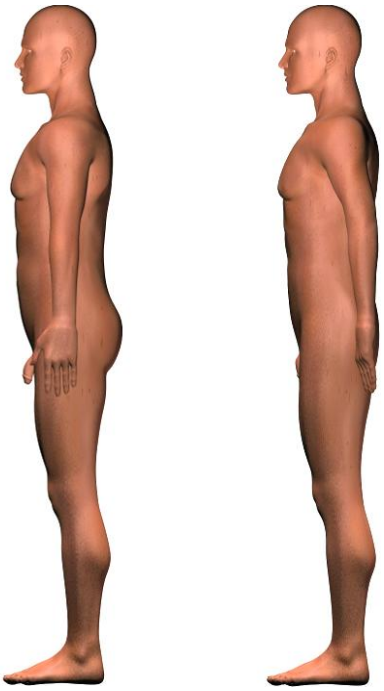

Figure 9. MASH2_sta and MASH2_sup: lateral view of surfaces

Smaller sagittal diameter, slightly greater lateral diameter, flatter breasts, broader shoulders and different positions of the arms are the external anatomical differences between standing and supine posture which catch the eye. The internal differences refer to the positions of organs which are shown for the MASH2_sta and the MASH2_sup phantoms for frontal and lateral views in figures 10a and 10b, respectively. The three horizontal lines facilitate the recognition of the organ shifts. Corresponding figures for the FASH2_sta and the FASH2_sup phantoms look quite similar because most organs and their relative positions are equal for males and females. The organ and tissue masses given in the appendix also apply to the supine phantoms, because only the positions of some organs were changed and adipose tissue was re-distributed without changing organ or tissue masses. The exception are the lungs, because their volume decreased in the supine phantoms by 8%, but this was compensated by an increase of the density by the same margin, which left the lungs mass unchanged.

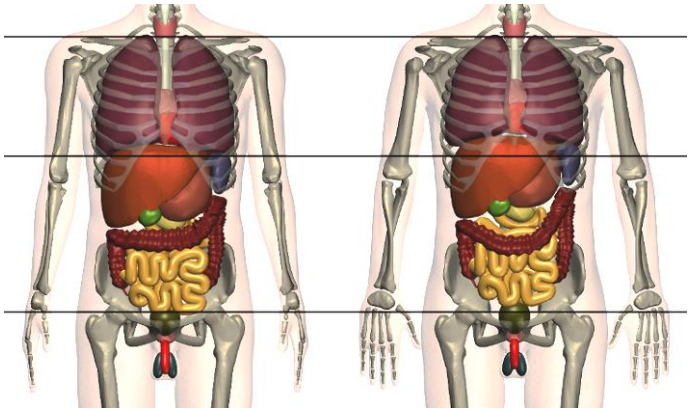

Figure 10a. MASH2_sta and MASH2_sup: Position of organs, frontal view

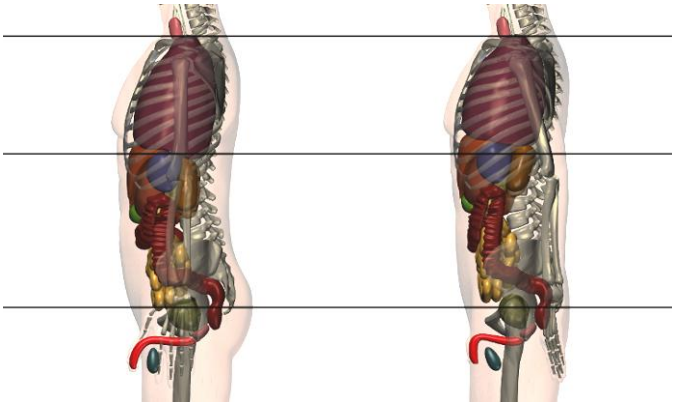

Figure 10b. MASH2_sta and MASH2_sup: Position of organs, lateral view

3.3 Organ and tissue absorbed doses for standing and supine posture

Most radiosensitive organs and tissues of the human body are located under layers of muscle and/or adipose tissue of varying thickness. For given external whole body exposure conditions, the thickness of overlying tissues becomes the influential parameter for the absorbed dose to organs and tissues because attenuation and scattering of photon radiation depends crucially on the distance between the surface, where the radiation enters the body, and the location of the organ in the direction of the beam, and also on the scatter properties of surrounding tissues, like bone structures, for example. Consequently, interpretation of organ and tissue absorbed doses in terms of the interaction between radiation field and human body can become quite a complex task to do.

X-ray diagnosis applies external partial body exposure to patients, which makes organ absorbed dose interpretation even more complicated, because now the positions of organs or tissues relative to the X-ray field may become even more important for the absorbed dose than the distance between surface and organ. Therefore, this study approaches the dosimetric results for X-ray examinations in two steps: First, whole body AP and PA exposure to monoenergetic photons will be considered for the standing and the supine phantoms. This allows for the investigation of the effect of posture-specific anatomical changes on organ and tissue absorbed doses and also for a comparison with corresponding data published by Sato et al (2008). Second, X-ray spectra, divergent beams, focus-to-detector distances and diagnostic field sizes will be introduced to calculate organ and tissue absorbed doses for radiographic examinations of the chest and the abdomen with all four phantoms, in order to investigate the combined effect of fat layer reduction, organ shift and position relative to the field boundary.

3.3.1 Whole body exposure

Whole body exposure with monoenergetic parallel photons, incident AP and PA on the MASH2_sta, the MASH2_sup, the FASH2_sta and the FASH2_sup phantoms have been simulated for energies between 10 keV and 10 MeV. The photon cut-off energy was 2 keV in all tissues, while electron histories were terminated at 5 keV in all skeletal tissues and at 20 keV in all tissues located outside the skeleton. Statistical errors varied between 0.2 and 3.5% depending on the size of the organ and the projection. Ratios between absorbed doses to selected organs and tissues of the supine and the standing phantoms are shown for the MASH2 phantom in table 4 for AP projection and for the FASH2 phantom in tables 5 for PA projection as a function of the photon energy. In each of the tables, the last line gives the sum of the statistical errors for the two phantoms averaged over all energies.

In tables 4 and 5 one finds 21 ratios being greater than unity, i.e. that the organ or tissue absorbed dose is greater for the supine posture than for the standing posture. 5 ratios are smaller than unity, i.e. that here the standing absorbed doses are greater than the supine absorbed doses. For the prostate AP a clear decision cannot be made within the margin of the statistical error. The greatest ratio is 4.8, found at 15 keV AP for the FASH2 colon, the smallest ratio is 0.5, found at 20 keV for the MASH2 kidneys. For AP and PA projection, Sato et al (2008b) reported for male phantoms a maximum ratio of 4.0 at 15 keV and a minimum ratio of 0.42 at 20 keV, without specifying the organ or tissue. Taking into account increasing statistical errors at low energies, the maximum and minimum ratios of Sato et al and from this study show good agreement. As the differences between absorbed doses for different postures are mostly caused by different thicknesses of adipose tissue located in front of the organ or tissue under consideration, the corresponding ratios can become quite large or small when the incident photon energy becomes smaller than 20 keV. However, the empty spaces in tables 4 and 5 for 10, 15 and 20 keV show that because of the strong increase of the statistical error with decreasing photon energy some of these very low energy ratios cannot reliably be determined.

Table 4. Ratios between organ and tissue absorbed doses for the MASH2_sup and the MASH2_sta phantoms for AP projection of a parallel beam of photons covering the whole body as function of the photon energy. Error (%) = sum of the statistical errors for both phantoms averaged over all energies.

E (MeV)	Bladder	Lungs	Colon	Liver	Kidneys	Spleen	Testes	Small Int.	Stomach	Thymus	Prostate	RBM	BSC
0.010							1.167						
0.015		2.250	2.471	1.606			1.012	1.667	1.263				1.500
0.020	1.621	1.466	1.528	1.211	0.500	0.817	1.027	1.444	1.074	2.601	1.000	1.186	1.273
0.030	1.258	1.151	1.162	1.058	0.825	0.950	1.010	1.219	1.024	1.346	1.053	1.105	1.124
0.040	1.118	1.086	1.096	1.031	0.901	0.985	1.048	1.153	1.019	1.135	1.055	1.065	1.064
0.050	1.159	1.064	1.079	1.022	0.919	0.970	0.995	1.100	1.012	1.084	1.090	1.044	1.026
0.060	1.120	1.053	1.061	1.015	0.951	0.989	1.019	1.094	1.010	1.070	1.126	1.044	1.032
0.070	1.090	1.039	1.049	1.016	0.946	0.977	1.096	1.068	0.990	1.046	1.033	1.040	1.028
0.080	1.047	1.041	1.048	1.010	0.941	0.998	1.030	1.080	1.018	1.068	1.054	1.040	1.035
0.100	1.063	1.031	1.044	1.012	0.955	0.997	1.044	1.066	0.999	1.059	1.060	1.033	1.031
0.150	1.052	1.031	1.044	1.013	0.970	0.990	1.100	1.061	1.012	1.042	1.073	1.032	1.022
0.200	1.080	1.031	1.039	1.012	0.976	0.967	1.042	1.064	1.003	1.055	1.064	1.032	1.029
0.300	1.088	1.032	1.047	1.004	0.979	0.985	1.033	1.059	1.006	1.092	0.952	1.028	1.020
0.500	1.001	1.029	1.029	1.016	0.953	0.964	0.977	1.047	0.982	1.071	0.978	1.028	1.020
1.000	1.045	1.001	1.025	1.000	0.960	1.016	0.934	1.027	1.000	1.013	1.036	1.028	1.017
3.000	1.003	1.010	0.992	0.989	0.982	0.994	1.037	1.040	1.030	1.009	1.109	1.015	1.013
6.000	0.923	1.008	1.022	1.006	0.985	0.974	1.066	1.032	0.972	1.105	1.183	1.004	1.001
10.00	1.004	0.991	0.999	0.985	0.981	0.984	0.974	1.021	0.957	0.946	0.977	1.014	0.998
Error (%)	3.0	1.0	1.0	0.6	1.6	1.8	3.6	1.0	1.6	3.6	5.8	1.0	1.0

Table 5. Ratios between organ and tissue absorbed doses for the FASH2_sup and the FASH2_sta phantoms for PA projection of a parallel beam of photons covering the whole body as function of the photon energy. Error (%) = sum of the statistical errors for both phantoms averaged over all energies.

E (MeV)	Adrenals	Colon	Uterus	Liver	Lungs	Kidneys	Spleen	Pancreas	Small Int.	Stomach	Ovaries	RBM	BSC
0.010													
0.015		4.800		0.800	0.625	2.079						1.500	1.000
0.020	0.543	2.000	2.176	0.979	0.741	1.354	0.583	2.048	3.000	1.235		1.116	1.038
0.030	0.785	1.346	1.486	1.000	0.872	1.133	0.822	1.432	1.604	1.204	1.936	1.081	1.056
0.040	0.889	1.195	1.389	1.009	0.913	1.081	0.911	1.305	1.309	1.165	1.592	1.056	1.031
0.050	0.929	1.153	1.275	1.026	0.934	1.061	0.946	1.250	1.221	1.196	1.499	1.042	1.020
0.060	0.961	1.114	1.261	1.015	0.954	1.064	0.973	1.227	1.181	1.163	1.339	1.041	1.031
0.070	0.960	1.097	1.221	1.023	0.953	1.050	0.954	1.193	1.154	1.133	1.185	1.037	1.033
0.080	0.965	1.088	1.216	1.025	0.965	1.063	0.953	1.201	1.148	1.109	1.251	1.032	1.024
0.100	1.011	1.082	1.216	1.028	0.962	1.044	0.962	1.174	1.114	1.094	1.206	1.032	1.017
0.150	0.944	1.090	1.197	1.023	0.962	1.033	0.968	1.136	1.118	1.118	1.187	1.022	1.015
0.200	0.988	1.098	1.220	1.024	0.968	1.049	0.961	1.165	1.108	1.111	1.243	1.028	1.017
0.300	1.033	1.079	1.201	1.017	0.977	1.049	0.981	1.146	1.121	1.074	1.230	1.024	1.012
0.500	1.002	1.084	1.146	1.012	0.981	1.044	0.990	1.117	1.088	1.064	1.177	1.022	1.022
1.000	1.107	1.045	1.139	1.005	0.988	1.019	1.007	1.112	1.082	1.035	0.984	1.008	1.007
3.000	0.945	1.029	1.020	1.009	0.995	1.014	0.993	1.073	1.043	1.004	1.210	0.991	0.992
6.000	1.133	1.031	1.086	1.001	0.994	1.028	0.999	1.072	1.027	1.090	1.045	0.998	1.001
10.00	0.998	0.989	1.016	1.007	1.007	0.992	0.990	1.077	1.031	1.028	0.945	1.004	1.003
Error (%)	4.6	1.2	3.6	0.8	0.6	1.0	1.8	2.6	1.6	2.0	6.9	0.8	0.8

If whole body exposure occurs, all organs and tissues are located inside the radiation field. Therefore, different subcutaneous fat layers of standing and supine phantoms are usually the explanation given for the ratios shown in tables 4 and 5. However, there are still two additional factors influencing the ratios between standing and supine organ and tissue absorbed doses: First, because of the gravitational force and of the cranial shifts, organs are also displaced in dorsal direction, as was shown in table 1, i.e. in the direction of the radiation beam for AP projection or towards the beam for PA projection, thereby either adding to the attenuation effect of the fat layer or (partly) compensating it. Second, the cranial shifts for supine posture push some organs (deeper) into the ribcage, thereby increasing the attenuation by bones, like ribs, sternum and scapulae. In other words, organ and tissue absorbed doses are the result of a superposition of attenuation effects caused by posture-specific subcutaneous fat layers and by organ positions. Some of the supine-to-standing absorbed dose ratios from tables 4 and 5 will be discussed based on transverse images of the organ under consideration.

The MASH2_sta and the MASH2_sup phantoms consist of 1462 transverse 2D images like those shown in figures 11a and 11b. The image count starts at the vertex of the phantom. Slice 500 of MASH2_sta represents also the centre slice for the liver. According to table 1, the cranial shift of the liver in the supine phantom is 1.7 cm, which corresponds to a shift by 1.7 cm / 0.12 cm = 14.2 slices. Consequently, for the liver slice 486 in the supine phantom corresponds anatomically to slice 500 in the standing phantom. In spite of the dorsal shifts shown in table 1, the AP ratios in table 4 for the liver and the stomach are greater than unity, because in the MASH2_sup phantom these organs are located closer to the frontal surface than in the MASH2_sta phantom. For the spleen the dorsal shift is similar but the ratio is smaller than unity, because the lateral shift of fat in the supine phantom increases the distance to the frontal surface. According to table 1, the kidneys were dorsally shifted by 1.2 cm in the supine MASH2 phantom, which more than compensates the shorter distance to the frontal surface and therefore the ratio for the kidneys is smaller than unity.

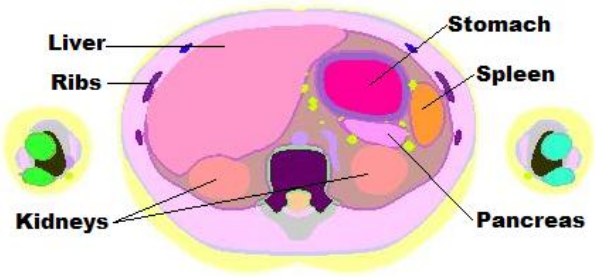

Figure 11a. MASH2_sta, slice 500

Figure 11b. MASH2_sup, slice 486

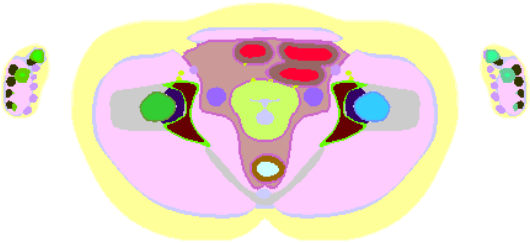

Figure 12a. FASH2_sta, slice 650

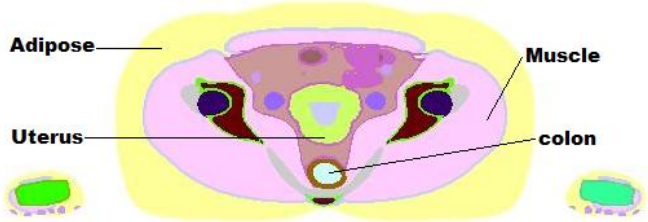

Figure 12b. FASH2_sup, slice 642

A strong increase of the absorbed dose to the uterus for PA projection can be seen for the supine posture from the ratio given in table 5. Figure 12b for the supine FASH2 phantom shows that the distance of the uterus to the rear surface of the body is significantly smaller than in the standing phantom shown in figure 12a. The comparison is made for the slices 650 and 642, because according to the cranial shift of 0.9 cm given in table 1, the difference between anatomically corresponding images for the uterus in both phantoms is 0.9 cm / 0.12 cm = 7.5 slices.

To analyze the absorbed dose to all segmented organs and tissues for the two phantoms and the two posture in this manner is beyond the scope of this paper. Also, external whole body irradiation is an exposure scenario more likely to be found in occupational radiation protection, where the effective dose is the quantity of primary interest. Figure 13 presents ratios between supine and standing effective doses for AP and PA projection as a function of the photon energy for the FASH2 and the MASH2 phantoms, as well as for the male adult supine phantom JM and standing phantom JM2 from Sato et al (2008b). Sato et al's effective doses are actually some kind of "male effective doses", because they used only male phantoms and did not include absorbed dose to the breasts. For incident photon energies above 30 keV, the differences between the effective doses for the two postures for all phantoms are smaller than 5%. Below 30 keV the FASH2/MASH2 ratios rapidly increase with decreasing energy, reflecting the majority of the ratios shown in tables 8 and 9 plus the effect of the high ICRP tissue weighting factors (ICRP 2007) for the breasts, colon, lungs and stomach. As for the JM/JM2 "male effective dose" ratio, initially one can see the same increase of the effective dose ratios but then for AP projection a decrease occurs between 15 and 10 keV, which probably is caused by the missing breast absorbed doses.

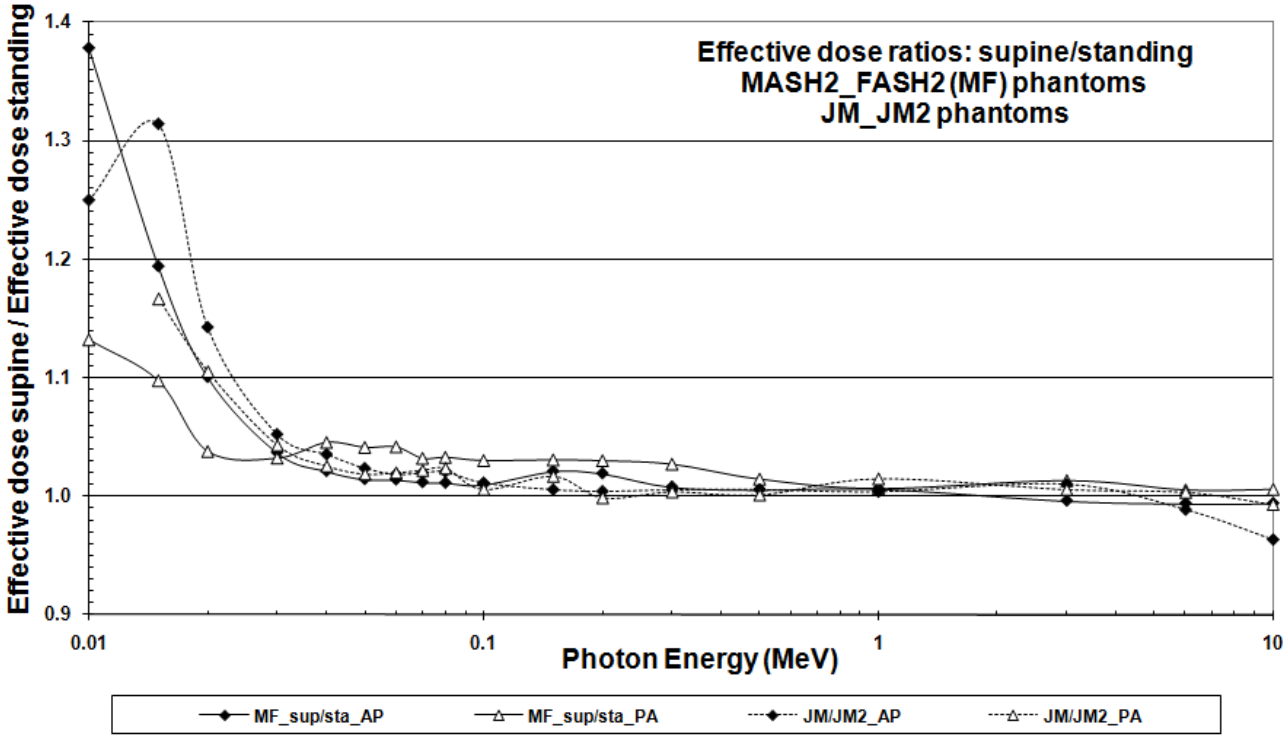

Figure 13. Ratios between supine and standing effective doses for AP and PA projection calculated with the (FASH2+MASH2)_sup and the (FASH2+ MASH2)_sta phantoms. Data from Sato et al (2008) for the Japanese male adult JM (supine) and JM2 (standing) phantoms are also shown.

3.3.2 X-ray exposure

The posture of the patient plays an important role in radiological protocols set up for examinations in X-ray diagnosis (Becht et al 2008, Bontrager 2003). Standing and supine postures are most frequently used for radiographs performed especially in the trunk region of the human body. With the FASH2_sta, the FASH2_sup, the MASH2_sta and the MASH2_sup phantoms, developed in this study, it is possible to investigate the effect of the posture on organ and tissue absorbed doses received by male and female adult patients undergoing X-ray examinations. This section will present posture-specific dosimetric data for radiographs of the thorax and the abdomen, because they belong to the most frequently performed procedures in X-ray diagnosis and because the large field size causes exposure to ionizing radiation for a significant number of radiosensitive organs and tissues. The quantity determined by the EGSnrc-based Monte Carlo code is the conversion coefficient (CC) D/INAK between organ or tissue absorbed dose D and incident air kerma (INAK) (ICRU 2005). The INAK is calculated free in air at the point where the central ray of the X-ray beam enters the patient. Photon and electron cut-off energies were the same used for whole body exposure. Absorbed doses were averaged over the volume of organs and tissues, except for the red bone marrow and the bone surface cells. For the two radiosensitive skeletal tissues, maximum absorbed doses among the bones located in the X-ray beam are given, a procedure already used before (Kramer et al 2008).

Apart from CCs D/INAK for selected organs and tissues exposed in abdominal and thoracic examinations, the following sections will present ratios between the supine and the standing CCs D/INAK, similar to the ratios presented for whole body exposure. Additionally, corresponding whole body ratios from tables 4 and 5 will be included based on the mean energy of the X-ray spectra used in the simulations. Partial body diagnostic X-ray exposure differs from the whole body exposure to

monoenergetic photons shown in the previous section mainly with respect to the energy distribution of the radiation and the type, the size and the location of the radiation field relative to the body surface. Applying the mean spectral energy to the monoenergetic data from tables 4 and 5 more or less eliminates the "energy-related difference". The "type-related difference", i.e. parallel field for whole body exposure versus divergent beam in X-ray diagnosis, can be neglected in a first approximation because not absolute absorbed doses but ratios of absorbed doses for the two types of exposure will be compared. Thus, primarily field size and field location are expected to make the difference between posture-specific organ and tissue absorbed dose ratios for whole body and X-ray exposure.

According to ICRP103 (ICRP 2007), the effective dose is not suitable for risk estimates for patients submitted to radiological examinations. Instead, a patient-specific risk evaluation should be made taking into account sex- and age-dependent risk coefficients for cancer incidence or mortality to be found in the BEIR VII report (National Research Council 2005), for example. Based on the concept of "whole body effective risk" proposed by D Brenner (Brenner and Huda 2008) and applied to medical exposure of patients earlier (Kramer et al 2008), risk estimates for cancer incidence for standing and supine posture will be calculated and compared for the X-ray examinations to be discussed in the next two section. The quantity to be determined is the number of cases for cancer incidence per 100000 exposed adult individuals. The sex- and age-dependent risk coefficients were taken from the BEIR VII report as quoted in table 2 of the study of Kramer et al (2008).

3.3.2.1 MASH2: Abdomen AP, supine

Apart from other diagnostic modalities, like ultrasound, CT or MR, a radiograph of the abdomen AP (ventro-dorsal) could be indicated in case of pain in that region, kidney or gall bladder colic or abdominal injuries, for example. Typically, the tube voltage is 90 kV, the filtration 2.5 mm Al, the focus-to-detector distance (FDD) 115 cm and the field size in the detector plane 35 cm x 40 cm. The patient is in supine position and the field is centred on the spine slightly above the navel (Becht et al 2008). Figure 14a shows this exposure scenario for the MASH2_sta phantom. The blue and the black fields represent the field size in image detector and entrance plane, respectively. The frontal and lateral views allow for easy recognition of organ positions relative to the X-ray beam. Figure 14b represents the abdominal examination as it should be simulated. Figure 14a applies to the case when a standing phantom has to be used because a supine phantom is not available. The exposure scenario is the same, except that organ positions relative to the X-ray field are different. The results of the Monte Carlo simulations for the two scenarios are shown in table 6 as CCs D/INAK for selected organs and tissues together with the statistical errors for the standing and the supine MASH2 phantom. Columns 6 and 7 of table 6 present ratios "Sup/Sta" between posture-specific results for the 35cm x 40cm field and for the whole body fields, respectively. The data for the whole body field where taken from table 4 and from the files with the complete whole body results (not shown here) for 45.9 keV, which is the mean photon energy of the X-ray spectrum used in the simulation. The differences between the ratios given in columns 6 and 7 are caused by the diagnostic field effect, which reflects the posture-specific change of the organ relative to the field boundaries, because the anatomical posture effect is already taken into account by the whole body ratio.

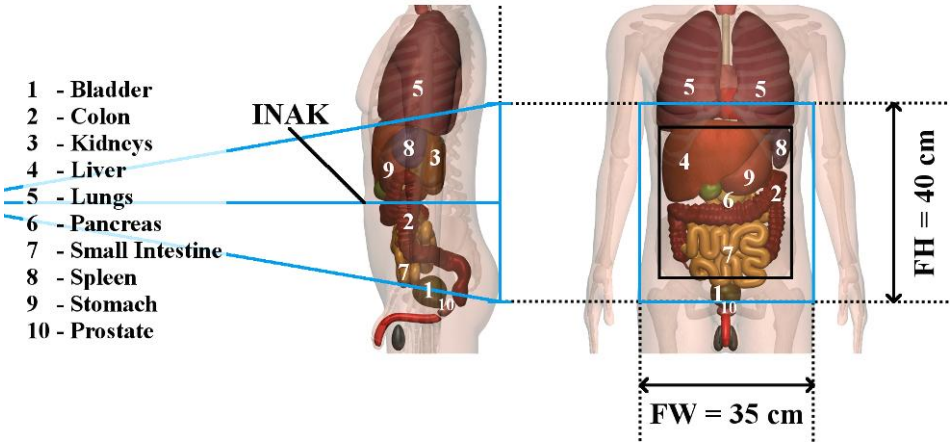

Figure 14a. Abdomen AP exposure scenario for the MASH2_sta phantom. FW = field width, FH = field height. Field size at image receptor in blue, at entrance in black.

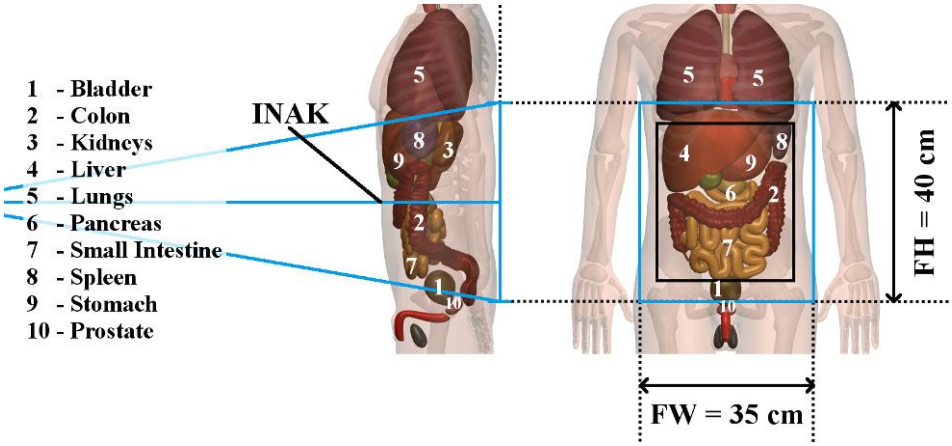

Figure 14b. Abdomen AP exposure scenario for the MASH2_sup phantom. FW = field width, FH = field height. Field size at image receptor in blue, at entrance in black.

The last column of table 6 shows that for whole body exposure with the mean spectral energy the urinary bladder wall and the small intestine wall receive 13.9% and 12.7% , respectively, more absorbed dose in supine posture compared to the standing posture due to the anatomical effect discussed above. However, for abdominal exposure with a diagnostic field of 35 cm x 40 cm these percentage differences rise to 48.9% and 25.2%, respectively, because of the posture-specific position of the organs relative to the radiation field: For supine posture, the urinary bladder and the small intestine move deeper into the X-ray beam and this increases the absorbed dose differences between supine and standing by 35% and 12.5%, respectively. The opposite situation concerns the liver. For whole body exposure the liver absorbed dose is 2.7% greater in supine than in standing posture. However, under abdominal X-ray exposure the supine liver absorbed dose becomes 3.2% smaller than the standing liver absorbed dose because under supine posture the liver moves partly out of the X-ray beam. Adrenals and prostate have combined statistical errors greater than the absorbed dose differences between supine and standing posture, which normally prohibits a sound dosimetric judgment. Nevertheless, the ratios for whole body and diagnostic exposure indicate that these two organs experience no additional diagnostic field effect. In figures 14a and 14b, the kidneys are located inside the beam volume, but for supine posture they are located cranially more towards the field

boundaries. Because of the divergent X-ray field, the fluence distribution has a maximum at the field centre and decreases towards the field boundaries, which causes the kidney absorbed dose for supine posture to decrease compared to the standing posture. Apart from the posture effect already seen for whole body exposure, almost no additional change due to the diagnostic X-ray field can be observed for colon, pancreas, spleen and stomach wall. 19.0% and 15.1% increase for supine RBM and BSC absorbed doses, respectively, is caused by less shielding by adipose layers in supine posture, because the skeleton did not move cranio-caudally with respect to the x-ray field during posture change. For this comparison, whole body data for RBM and BSC are not available, because the whole body calculations determine the average absorbed dose in the whole skeleton but not the maximum absorbed dose in a single bone.

Table 6. Conversion coefficients between selected organ and tissue absorbed doses D and incident air kerma INAK for abdominal radiographs AP simulated with the MASH2_sta and the MASH2_sup phantoms. Ratios between supine and standing CCs are given for the X-ray field and for whole body exposure taken from table 4 for the mean spectral energy of 45.9 keV.

MASH2 Abdomen AP, 35cm x 40cm 90 kV, 2.5 mm Al, FDD = 115 cm	Standing D/INAK Gy/Gy	Standing Error %	Supine D/INAK Gy/Gy	Supine Error %	Sup/Sta Field 35 x 40	Sup/Sta Field wb*
ADRENALS	0.129	3.1	0.123	3.2	0.953	0.962
URINARY BLADDER WALL	0.090	1.9	0.134	1.6	1.489	1.139
COLON WALL	0.443	0.3	0.514	0.3	1.160	1.088
KIDNEYS	0.155	0.6	0.136	0.7	0.877	0.910
LIVER	0.504	0.1	0.488	0.2	0.968	1.027
PANCREAS	0.417	0.6	0.486	0.5	1.165	1.123
SMALL INTESTINE WALL	0.393	0.3	0.492	0.2	1.252	1.127
SPLEEN	0.328	0.6	0.319	0.6	0.973	0.978
STOMACH WALL	0.587	0.4	0.591	0.4	1.007	1.015
PROSTATE	0.021	6.9	0.022	6.8	1.048	1.073
RED BONE MARROW (max.)	0.079	1.2	0.094	1.1	1.190	
BONE SURFACE CELLS (max.)	0.119	1.4	0.137	1.3	1.151	

wb*: whole body, mono-energetic for 45.9 keV

The risk calculation for the abdominal AP exposure shown in table 6 assumes a 40-year-old male patient and an INAK of 5 mGy. Following the method outlined in Kramer et al (2008), the results for the risk of cancer incidence from the abdominal X-ray exposure are 7.4 cases and 8.1 cases per 100000 exposed individuals for the standing and the supine posture, respectively, i.e. a risk difference of 9.5%

3.3.2.2 FASH2: Thorax PA, standing

Perhaps one of the most frequently performed examination is a radiograph of the thorax PA (dorso-ventral) to investigate the conditions of the heart and the lungs. A typically used tube voltage is 125 kV, the filtration 2.5 mm Al, the FDD = 180 cm and the field size in the image receptor plane 35 cm x 40 cm. The patient is in standing position and the field is centred on the spine between the 6^{th} and 7^{th} thoracic vertebrae (Becht et al 2008, Bontrager 2003). Figures 15a and 15b show the exposure scenarios for the standing and the supine FASH2 phantoms and table 7 present the results. Whole body exposure data were taken from table 5 and from the files with the complete whole body results (not shown here) for 55.3 keV, which is the mean photon energy of the X-ray spectrum used in the simulation.

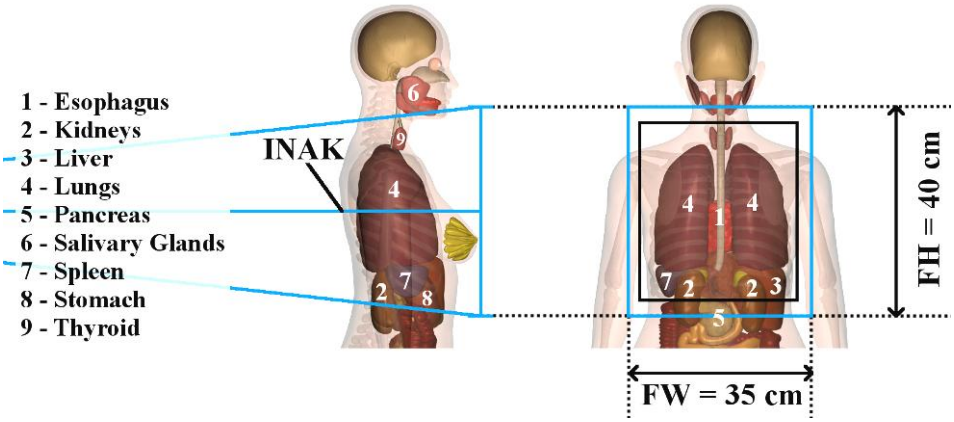

Figure 15a. Thorax PA exposure scenario for the FASH2_sta phantom. FW = field width, FH = field height. Field size at image receptor in blue, at entrance in black.

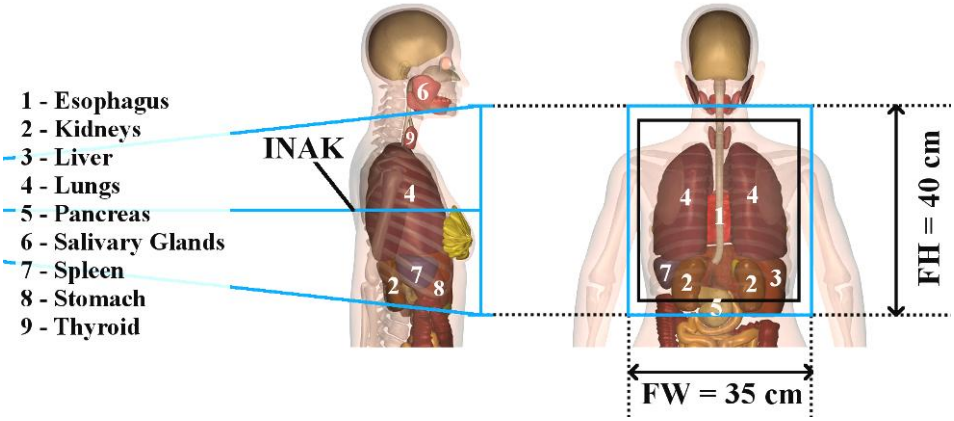

Figure 15b. Thorax PA exposure scenario for the FASH2_sup phantom. FW = field width, FH = field height. Field size at image receptor in blue, at entrance in black.

Figures 15a and 15b show that the organs shifted deeper into the X-ray beam in supine posture are the kidneys, pancreas, liver and stomach. Consequently, their supine/standing ratios for the diagnostic field in table 7 show increase of absorbed dose by 58.9%, 60.9%, 12.6% and 25.4%, respectively. The supine absorbed dose for the spleen is smaller than for standing posture for reasons mentioned already in the discussion of figure 11, which concerned the fat distribution versus the dorsal shift and has nothing to do with the relative position to the X-ray field. Consequently, the spleen ratios for whole body and diagnostic field are essentially equal. For the adrenals the combined statistical error of 3.5% is twice the percentage difference between the whole body and diagnostic field ratios, which make it impossible to come to a clear decision as to the cause for the difference. Figures 15a and 15b show the thyroid located at the same position relative to the X-ray field for both postures and the difference of 4.2% between the whole body and the diagnostic field ratios is smaller than the combined statistical error of 4.6%. Therefore, the difference between the posture-specific thyroid absorbed doses can be considered as statistical uncertainty. The lungs absorbed dose is almost 5% smaller for the supine posture than the for the standing posture. The lateral views of figures 15a and 15b show more overlying tissue in front of the lower dorsal part of the lungs for the supine posture, because 8% of their volume has been removed. This explains the observed difference between the posture-specific lungs absorbed doses. The lungs ratio for whole body exposure agrees within 0.8% with the diagnostic field ratio because the lungs are completely inside the X-ray field and

were not shifted. Another organ probably not affected by the change of posture is the oesophagus. The difference between the oesophagus absorbed doses for the two postures is only 1% and well below the combined statistical error of 2.8%. For supine posture, RBM and BSC show smaller increase in absorbed dose compared to the abdominal AP exposure in table 6 because the reduction of the SAD is smaller in the area of the ribcage compared to the abdominal region.

Table 7. Conversion coefficients between selected organ and tissue absorbed doses D and incident air kerma INAK for thoracic radiographs PA simulated with the FASH2_sta and the FASH2_sup phantoms. Ratios between supine and standing CCs are given for the X-ray field and for whole body exposure taken from table 5 for the mean spectral energy of 55.3 keV.

FASH2 Thorax PA, 35cm x 40cm 125 kV, 2.5mm Al, FDD = 180 cm	Standing D/INAK Gy/Gy	Standing Error %	Supine D/INAK Gy/Gy	Supine Error %	Sup/Sta Field 35 x 40	Sup/Sta Field wb*
ADRENALS	0.647	1.7	0.622	1.8	0.961	0.945
KIDNEYS	0.523	0.4	0.831	0.4	1.589	1.063
LIVER	0.317	0.3	0.357	0.3	1.126	1.020
LUNGS	0.631	0.2	0.601	0.2	0.952	0.944
OESOPHAGUS	0.399	1.4	0.395	1.4	0.990	0.972
PANCREAS	0.169	1.2	0.272	0.9	1.609	1.239
SPLEEN	0.489	0.7	0.474	0.7	0.969	0.960
STOMACH WALL	0.256	0.9	0.321	0.8	1.254	1.180
THYROID	0.304	2.3	0.284	2.3	0.934	0.973
RED BONE MARROW (max.)	0.633	1.5	0.656	1.5	1.036	
BONE SURFACE CELLS (max.)	0.894	2.3	0.932	2.2	1.043	

wb*: whole body, mono-energetic for 55.3 keV

Risk estimates for the thoracic PA examination shown in table 7, for a 40-year-old female patient and an INAK of 2.5 mGy give 7.7 and 7.8 cases per 100000 exposed individuals for standing and for supine posture, respectively, i.e. a risk difference of 1.3%

4. Conclusions

FASH2 and MASH2 are mesh-based adult phantoms modelled in standing and supine postures. Compared to the work of Sato et al (2007, 2008a, b), who CT-scanned a volunteer in standing and in supine posture, this study had to choose a different method to develop posture-specific human phantoms, because the standing FASH2_sta and MASH2_sta phantoms were not based on images of persons. The FASH2_sta and the MASH2_sta phantoms have been developed based on anatomical atlases (Cassola et al 2010), which show human anatomy in standing posture but not in supine posture. Therefore, for the development of phantoms in supine posture it was necessary to find anthropometric data in scientific publications which describe quantitatively the changes affecting organ positions, fat layer thickness, lungs volume, etc. to provide a data base to be used for the modelling of the supine phantoms FASH2_sup and MASH2_sup. Fortunately, the anthropometric data necessary for the modelling of the supine phantoms could be found, whereby it became possible to model anatomically realistic phantoms in supine posture.

In this study, posture-specific organ and tissue absorbed doses and ratios between them for exposure to external photon radiation have been presented for whole body and for diagnostic X-ray irradiation simulating AP and PA projections. For whole body exposure, differences between standing and supine organ doses depend primarily on dorsal organ shifts plus changes of the fat layer thickness.

Cranial organ shifts add to the absorbed dose differences only when posture change alters the shielding by bones (ribs, sternum and scapulae) for the organ under consideration. Additionally, cranial shifts of organs play a major role for X-ray exposure because of the limited field size. Cranial displacement into or out of the radiation beam are often responsible for the main part of the difference found between organ absorbed doses for standing and supine posture.

The dosimetric results for whole body exposure confirm data published by Sato et al (2008b). Maximum and minimum ratios between organ and tissue absorbed doses for supine and standing posture show similar values in both studies. There is also agreement that for whole body exposure with AP and PA projections posture-specific changes of the effective dose remain below 5% for incident photon energies above 30 keV. In Sato et al's paper this result was also confirmed for lateral, rotational and isotropic radiation fields. Consequently, in occupational radiation protection the supine posture is hardly a relevant issue, because a supine posture of the exposed individual and photon energies below 30 keV for whole body exposure are rare to be found.

Supine posture is a frequent position for exposed patients, not only in X-ray diagnosis but also in other areas of radiology, and in nuclear medicine and radiotherapy as well. Therefore, it is warranted to have both types of phantoms, standing and supine, available for dosimetric simulations of medical procedures. As for the two X-ray radiographs considered in this study, organ and tissue absorbed doses between supine and standing posture showed differences up to 60%, which is not a margin to be ignored. Routine occupational radiation protection can do most of its job only by looking at the effective dose, but in radiation protection in medicine knowledge of organ and tissue absorbed doses is still necessary because of the dose levels and resulting radiation risks involved.

Whole body risk for cancer incidence was calculated for the two radiographs based on data given in the BEIR VII report (National Research Council 2005). The differences between the risks for supine and standing posture were 9.5% and 1.3% for the abdominal and for the thoracic radiograph, respectively. These differences may seem to be small, but one should not forget that the selected X-ray examinations are just two out of many procedures performed in X-ray diagnosis every day. In view of a world-wide trend towards increasing body mass among human populations, the modelling of human phantoms reflecting this trend has become a necessity and will be the focus of a follow-up project to this study. FASH2 and MASH2 have body masses based on ICRP89 (ICRP 2002), while statistical data from around the world indicate that the 50^{th} body mass percentiles for adult males and females are meanwhile 5-6 kg greater than the ICRP89 reference whole body masses. One can expect the posture-specific differences between organ and tissue absorbed doses and consequently also between associated radiation risks to increase when phantoms representing patients with greater body mass will be modelled and used in the simulations. The difference between standing and supine SAD, a parameter crucial for organ and tissue absorbed doses in AP or PA projection, will certainly increase with body mass, for example.

Like the FAX06 and MAX06 phantoms, developed earlier by the research group of the Federal University of Pernambuco (Kramer et al 2006), the FASH2 and the MASH2 posture-specific phantoms are available for the scientific community. For downloading the phantoms one has to go to www.grupodoin.com and click on the link "Caldose" on the right side of the page.

5. Acknowledgements

The authors would like to thank the Conselho Nacional de Desenvolvimento Científico e Tecnológico - CNPq and the Fundação de Amparo à Ciência do Estado de Pernambuco - FACEPE for financial support.

6. Appendix

Tables A1 and A2 show theoretical skeletal volumes based on ICRP89 (2002) and ICRP70 (1995) calculated for cortical bone, spongiosa and the medullary cavities and the actually segmented volumes for the FASH/FASH2_sta and the MASH/MASH2_sta phantoms, respectively. The data for FASH and MASH were taken from the paper of Cassola et al (2010). The bold, italic numbers represent volumes which deviate more than 10% from the ICRP-based data. The tables show that the approximation between the skeletal tissue volumes of the phantoms and the ICRP-based data improved, not only for the "more than 10% deviators", but also for all other skeletal regions.

All segmented organ and tissue masses of the FASH2_sta and the MASH2_sta phantoms are shown in tables A3 and A4, respectively, together with the ICRP89 reference masses and corresponding data for the FASH or the MASH phantoms. Differences between FASH/MASH phantom masses and ICRP89 masses were smaller than 2.6%, except for the skeleton and the lymphatic nodes (Cassola et al 2010). Now, all differences are below 0.5%, except for the masses of the skeleton and the lymphatic nodes. The ICRP89 reference mass for cartilage includes also cartilage which is located outside the skeleton (nose, ears, thyroid, etc.). In tables A3 and A4, the skeleton masses for all phantoms include only the cartilage mass actually segmented in the skeletons, which is about 70% of the ICRP reference mass. A similar situation exists for the lymphatic nodes, a part of which, according to ICP89, is located in the bone marrow. Therefore, only 50% of the reference mass for the lymphatic nodes have been segmented in the FASH2_sta and the MASH2_sta phantoms.

Table A1. Theoretically calculated and actually segmented female skeletal tissue volumes

	ICRP-based	FASH	FASH2	ICRP-based	FASH	FASH2	ICRP-based	FASH	FASH2
Skeletal region	Cortical bone (cm^3)	Cortical bone (cm^3)	Cortical bone (cm^3)	Spongiosa (cm^3)	Spongiosa (cm^3)	Spongiosa (cm^3)	Med. cavity (cm^3)	Med. cavity (cm^3)	Med. cavity (cm^3)
Hands	61.1	61.1	61.2	41.3	41.6	41.3			
Radii and Ulnae	56.8	57.6	56.8	60.0	59.3	60.0	38.4	38.4	38.4
Humeri	51.2	51.7	51.2	150.3	150.1	150.3	57.6	57.4	57.6
Ribs	83.9	***139.9***	***131.1***	206.3	***154.9***	***162.2***			
Sternum	20.1	19.9	20.1	40.0	41.4	40.0			
Scapulae	63.6	65.8	63.6	68.5	70.8	68.6			
Clavicles	12.7	12.6	12.6	22.0	22.2	22.0			
Cervical vertebrae	19.7	***26.3***	***26.2***	107.9	***65.8***	***85.7***			
Thoracic vertebrae	38.9	***75.0***	***61.1***	317.7	293.8	292.4			
Lumbar vertebrae	47.2	***63.5***	46.8	245.2	259.8	244.5			
Sacrum	45.3	45.4	45.3	138.7	139.9	138.7			
Cranium	308.3	311.7	308.3	191.0	191.6	191.0			
Mandible	30.7	31.8	30.7	20.0	20.0	20.0			
Pelvis	180.1	185.2	180.1	338.5	350.1	338.5			
Femora	156.8	154.0	156.8	505.1	518.9	505.1	198.3	198.7	198.3
Patellae	11.7	11.6	11.6	14.5	14.6	14.5			
Tibiae and fibulae	198.0	195.8	198.0	230.5	230.1	230.5	132.2	132.2	132.2
Feet	181.8	180.4	181.8	99.8	100.0	99.8			
Total volume	1567.8	1689.3	1643.3	2797.5	2724.9	2705.1	426.5	426.7	426.5

Table A2. Theoretically calculated and actually segmented male skeletal tissue volumes

	ICRP-based	MASH	MASH2	ICRP-based	MASH	MASH2	ICRP-based	MASH	MASH2
Skeletal region	Cortical bone (cm^3)	Cortical bone (cm^3)	Cortical bone (cm^3)	Spongiosa (cm^3)	Spongiosa (cm^3)	Spongiosa (cm^3)	Med. Cavity (cm^3)	Med. Cavity (cm^3)	Med. Cavity (cm^3)
Hands	79.7	78.9	79.7	54.7	54.9	54.8			
Radii and Ulnae	86.5	86.4	86.5	93.8	94.5	93.8	59.0	59.1	59.0
Humeri	86.0	85.7	86.0	214.7	216.0	214.8	89.9	89.8	89.9
Ribs	183.9	***204.7***	183.9	273.0	260.2	273.0			
Sternum	28.8	28.8	28.8	52.2	52.3	52.2			
Scapulae	120.4	120.2	120.4	91.4	91.5	91.4			
Clavicles	22.4	22.4	22.4	29.0	29.2	29.0			
Cervical vertebrae	23.9	***51.5***	***32.4***	134.8	***103.3***	124.0			
Thoracic vertebrae	47.7	***120.2***	***64.9***	404.5	***338.7***	386.3			
Lumbar vertebrae	58.1	***81.7***	58.1	312.5	292.7	312.5			
Sacrum	65.1	64.9	65.1	182.3	182.1	182.3			
Cranium	422.2	417.6	422.2	249.4	250.4	249.4			
Mandible	42.5	42.0	42.5	26.2	25.8	26.2			
Pelvis	259.9	257.9	259.9	443.1	443.1	443.1			
Femora	197.7	199.7	197.7	667.1	667.5	667.2	277.4	277.1	277.4
Patellae	19.1	19.0	19.1	22.0	22.0	22.0			
Tibiae and fibulae	241.0	245.7	241.0	321.5	321.2	321.4	184.8	184.0	184.8
Feet	221.3	219.4	221.3	143.9	145.3	145.1			
Total volume	2206.0	2346.7	2231.9	3715.9	3590.7	3688.5	611.1	610.0	611.1

Table A3. Female organ/tissue masses from ICRP89, for the FASH and the FASH2_sta voxelized phantoms

ADULT FEMALE ORGAN / TISSUE	ICRP89 [g]	FASH [g]	FASH2 [g]	FASH2 / ICRP89 [%]
Adrenals	13.0	13.3	13.0	
Salivary Glands	70.0	69.2	70.0	
Oesophagus	35.0	34.3	35.0	
Stomach wall	140.0	140.0	140.0	
Small Intestine wall	600.0	599.3	600.0	
Colon wall	360.0	355.7	360.0	
Liver	1400.0	1400.0	1400.0	
Gallbladder wall	8.0	8.2	8.0	
Pancreas	120.0	118.8	120.0	
Brain	1300.0	1283.6	1300.0	
Breasts, glandular	200.0		200.0	
Breasts, adipose	300.0		300.0	
Breasts, total		501.0		
Heart wall	250.0	252.2	250.0	
Adipose	18700.0	19053.4	18698.1	0.01
Skin	2300.0	2303.4	2308.9	0.4
Muscle	17500.0	17493.4	17493.2	-0.04
Lungs	950.0	946.6	950.0	
Skeleton	7800.0	7343.4	7389.9	-5.3
Spleen	130.0	130.0	130.0	
Thymus	20.0	20.0	20.0	
Thyroid	17.0	16.8	17.0	
Kidneys	275.0	275.0	275.0	
Bladder wall	40.0	39.7	40.0	
Ovaries	11.0	11.0	11.0	
Uterus	80.0	80.0	80.0	
	52619.0	52488.3	52209.1	-0.8
Tongue	60.0	73.0	60.0	
Larynx	19.0			
Extra thoracic airw.		94.1	91.5	
GI content	830.0	710.0	830.5	0.06
Gall bladder content	48.0	41.2	48.0	
Trachea	8.0	8.6	8.0	
Tonsils	3.0			
Ureter/Urethra	18.0			
Fallopian Tubes	2.1			
Pituary Gland	0.6			
Eyes	15.0	16.5	15.0	
Optic nerve				
Blood	3570*			
Spinal chord		70.9	54.3	
	57192.7	53502.6	53316.4	-6.8
Connective Tissue	2100.0			
Lymphatic Nodes	600.0	298.7	300.0	-50.0
	59892.7	53801.3	53616.4	-10.5
Other tissues		6295.7**	6420.5**	
Total mass	59892.7	60097.0	60036.9	0.2
Height	163 cm	162.5 cm	162.5	-0.3

* without lungs

** includes blood, connective tissue, non-articular cartilage and other soft tissue, etc.

Table A4. Male organ/tissue masses from ICRP89, for the MASH and the MASH2_sta voxelized phantoms

MALE ADULT ORGAN / TISSUE	ICRP89 [g]	MASH [g]	MASH2 [g]	MASH2 / ICRP89 [%]
Adrenals	14.0	14.0	14.0	
Salivary Glands	85.0	83.7	85.0	
Oesophagus	40.0	45.2	40.0	
Stomach wall	150.0	148.5	150.0	
Small Intestine wall	650.0	652.8	650.0	
Colon wall	370.0	366.7	370.0	
Liver	1800.0	1800.0	1800.0	
Gallbladder wall	10.0	10.0	10.0	
Pancreas	140.0	140.0	140.0	
Brain	1450.0	1438.2	1450.0	
Breasts, glandular	10.0		10.0	
Breasts, adipose	15.0		15.0	
Breasts, total		24.7		
Heart wall	330.0	332.0	330.0	
Adipose	14500.0	14565.6	14518.9	0.10
Skin	3300.0	3311.9	3301.0	0.03
Muscle	29000.0	29001.1	29000.0	
Lungs	1200.0	1181.5	1200.0	
Skeleton	10500.0	9894.9	9950.5	-5.2
Spleen	150.0	150.0	150.0	
Thymus	25.0	24.8	25.0	
Thyroid	20.0	20.1	20.0	
Kidneys	310.0	310.0	310.0	
Bladder wall	50.0	50.0	50.0	
Testes	35.0	35.2	35.0	
Prostate	17.0	17.1	17.0	
	64146.0	63618.0	63641.4	-0.8
Tongue	73.0	39.4	73.0	
Larynx	28.0			
Extra thoracic airw.		121.2	107.9	
GI content	900.0	964.4	901.5	0.2
Gall bladder cont.	58.0	55.8	58.0	
Trachea	10.0	12.8	10.0	
Tonsils	3.0			
Ureter/Urethra	26.0			
Epididymes	4.0			
Pituary Gland	0.6			
Eyes	15.0	16.2	15.0	
Optic nerve				
Blood	4900*			
Spinal chord		113.7	111.5	
	70188.6	64941.5	64918.3	-7.5
Connective Tissue	2600.0			
Lymphatic Nodes	730.0	350.0	360.1	-50.7
	73518.6	65291.5	65278.4	-11.2
Other tissues		7491.9**	7422.1**	
Total mass	73518.6	72783.4	72700.5	-1.1
Height	176 cm	175.6 cm	175.6 cm	-0.2

* without lungs

** includes blood, connective tissue, non-articular cartilage and other soft tissue, etc

7. References

Akahane K, Kai M, Kusama T and Saito K 2001 Dose estimation of patients from diagnostic X-ray based on CT-voxel phantom, *Proceedings of the Ninth EGS4 Users' Meeting in Japan, KEK Proceedings 2001-22, 87-91*

Albert R K and Hubmayr R D 2000 The Prone Position Eliminates Compression of the Lungs by the Heart, *Am J Respir Crit Care Med* **161** 1660-1665

Ball W S, Wicks J D and Mettler, Jr. F A 1980 Prone-supine Change in Organ Position: CT Demonstration, *American Journal of Roentgenology* **135** 815-820

Bauer J 2010 private communication: email from March 26, Institut für Röntgendiagnostik of the Technische Universität Muenchen, Germany

Becht S, Bittner R C, Ohmstede A, Pfeiffer A and Rossdeutscher R 2008 Lehrbuch der röntgendiagnostischen Einstelltechnik, 6. Auflage, *Springer Medizin Verlag*, Heidelberg

Bein T 2010 private communication: email from March 21, Klinikum of the University of Regensburg, Germany

Blair E and Hickam J B 1955 The Effect of Change in Body Position on Lung Volume and Intrapulmonary Gas Mixing in Normal Subjects, *J Clin Invest* **34** No.3 383-389

Blender 2009 http://www.blender.org/ Last access December 2009

Bontrager K L 2003 Tratado de Técnica Radiológica e Base Anatómica, *Guanabara Koogan*, Rio de Janeiro

Bozkurt A and Bor D 2007 Simultaneous determination of equivalent dose to organs and tissues of the patient and of the physician in interventional radiology using the Monte Carlo method, *Phys Med Biol* 52 317-330

Brenner D and Huda W 2008 Effective Dose: A Useful Concept in Diagnostic Radiology *Rad Prot Dos* **128**(4) 503-508

Cassola V F, de Melo Lima V J, Kramer R and Khoury H J 2010 FASH and MASH: Female and Male Adult human phantoms based on polygon meSH surfaces. Part I: Development of the anatomy *Phys Med Biol* **55** 133-162

Drexler G Panzer W Widenmann L Williams G and Zankl M 1990 The Calculation of Dose from External Photon Exposures Using Reference Human Phantoms and Monte Carlo Methods, Part III: Organ Doses in X-Ray Diagnosis, Institut für Strahlenschutz, GSF- Gesellschaft für Umwelt und Gesundheit, D-8042 Neuherberg, *GSF-Bericht S-11, revised and amended version of S-1026, 1984*

Dimbylow P and Findlay R 2010 The effects of body posture, anatomy, age and pregnancy on the calculation of induced current densities at 50 Hz, *Rad Prot Dos* 139(4) 532-538

Feig S A 1980 Biological determinants of radiation-induced human breast cancer, *Crit Rev Diagn Imaging* 13(3) 229-248

Findlay R P and Dimbylow P J 2005 Effect of posture on FDTD calculations of specific absorption rate in a voxel model of the human body, *Phys Med Biol* **50** 3825-3835

Hart D Jones D G and Wall B F 1994 Estimation of Effective Dose in Diagnostic Radiology from Entrance Surface Dose and Dose-Area Product Measurements, *National Radiological Protection Board,* Chilton, Didcot, Oxon OX11 0RQ, UK, NRPB-R262

ICRP 1995 Basic Anatomical and Physiological Data for use in Radiological Protection: The Skeleton. *ICRP Publication 70* (Oxford: Pergamon)

ICRP 1996 Conversion Coefficients for use in Radiological Protection against External Radiation. *ICRP Publication 74*. (Oxford: Pergamon)

ICRP 2002 Basic Anatomical and Physiological Data for Use in Radiological Protection: Reference Values *ICRP Publication 89* (Oxford: Pergamon)

ICRP 2004 Dose to Infants from Ingestion of Radionuclides in Mother's Milk *ICRP Publication 95 Ann ICRP 34 (3-4)* Elsevier Science Ltd., Oxford

ICRP 2007 Recommendations of the International Commission on Radiological Protection *ICRP Publication 103 Ann. ICRP 37 (2-3) Elsevier Science Ltd., Oxford*

ICRP 2009 Adult Reference Computational Phantoms *ICRP Publication 110 Ann. ICRP 39 (2-3) Elsevier Science Ltd., Oxford*

ICRU 1992 Photon, Electron, Proton and Neutron Interaction Data for Body Tissues *ICRU Report No. 46* International Commission On Radiation Units And Measurements, Bethesda, MD, USA

ICRU 2005 Patient dosimetry for X-rays used in medical imaging *ICRU Report No. 74* International Commission On Radiation Units And Measurements, Bethesda, MD, USA

ImageJ 2009 National Institute of Health. ImageJ: Image Processing and Analysis in Java http://rsbweb.nih.gov/ij/index.html Last access December 2009

Iribarren C, Darbinian J A, Lo J C, Fireman B H and Go A S 2006 Value of the Sagittal Abdominal Diameter in Coronary Heart Disease Risk. Assessment: Cohort Study in a large, Multiethnic Population, *Am J of Epidemiol* **164**, No.12 1150-1159

Johnson P, Lee C, Johnson K, Siragusa D and Bolch W 2009 The influence of patient size on dose conversion coefficients: a hybrid phantom study for adult cardiac catheterization *Phys Med Biol* **54** 3613-3629

Jones D G and Wall B F 1985 Organ Doses from Medical X-ray Examinations Calculated Using Monte Carlo Techniques, *National Radiological Protection Board*, Chilton, Didcot, Oxon OX11 0RQ, UK, NRPB-R186

Kawrakow I 2000a Accurate condensed history Monte Carlo simulation of electron transport. I. EGSnrc, the new EGS4 version, *Med Phys* **27**, 485-498

Kawrakow I 2000b Accurate condensed history Monte Carlo simulation of electron transport. II. Application to ion chamber response simulations, *Med Phys* **27**, 499-513

Kawrakow I and Rogers D.W.O. 2003 The EGSnrc code system: Monte Carlo simulation of electron and photon transport, *NRC Report PIRS-701*

Kramer R and Drexler G 1976 Zum Verhältnis von Oberflächen- und Körperdosis in der Röntgendiagnostik, 7. Wissenschaftliche Tagung der Deutschen Gesellschaft für

Medizinische Physik e.V. Heidelberg, 5.-7.5.1976, In: *Medizinische Physik*, Band 2, p. 683-695, Herausgegeben von W. J. Lorenz, Hüthig Verlag, Heidelberg.

Kramer R, Khoury H J, Vieira J W and Kawrakow I 2006 Skeletal dosimetry in the MAX06 and the FAX06 phantoms for external exposure to photons based on vertebral 3D-microCT images *Phys.Med.Biol.* **51** 6265-6289

Kramer R, Khoury H J and Vieira J W 2008 CALDose_X a software tool for the assessment of organ and tissue doses, effective dose and cancer risk in diagnostic radiology *Phys Med Biol* **53** 6437-6459

Kramer R, Cassola V F, Khoury H J, Vieira J W, de Melo Lima V J and Robson Brown K 2010 FASH and MASH: female and male adult human phantoms based on polygon mesh surfaces: II. Dosimetric calculations, *Phys Med Biol* **55** 163-189

Le Heron J C 1992 Estimation of effective dose to the patient during medical x-ray examinations from measurements of the dose-area product, *Phys Med Biol* **37** 2117-2126

Liu H, Gu J, Caracappa P F and Xu X G 2010 Comparison of two types of adult phantoms in terms of organ doses from diagnostic CT procedures, *Phys Med Biol* **55** 1441-1451

MakeHuman 2009 http://www.makehuman.org/blog/index.php Last access June 2009

Min P 2009 Binvox: 3D mesh voxelizer, http://www.google.com/search?q=binvox Last access June 2009

Nagaoka T and Watanabe S 2008 Postured voxel-based human models for electromagnetic dosimetry, *Phys Med Biol* **53** 7047-7061

National Research Council 2005 Health Risks from Exposure to Low Levels of Ionizing Radiation – BEIR VII. *The National Academies Press*, Washington DC

Noorudin F and Turk G 2003 Simplification and repair of polygonal models using volumetric techniques *IEEE Trans. Vis. Comput. Graphics* **9** 191–205

Ochs-Balcom H M, Grant B J B, Muti P, Sempos C T, Freudenheim J L, Trevisan M, Cassano P A, Iacoviello L and Schünemann H J 2006 Pulmonary Function and Abdominal Adiposity in the Genaral Population, *CHEST* **129** No.4 853-862

Petoussi-Henss N Panzer W Zankl M and Drexler G 1995 Dose-Area Product and Body Doses, *Rad Prot Dos* **57** Nos 1-4, 363-366

Petoussi-Henss N Zankl M and Panzer W 2005 Estimation of organ doses in radiology using voxel models describing different patients, *Biomedizinische Technik*, Vol 50, Supplementary volume 1, Part 1, 664-665

Reiff J E, Werner-Wasik M, Valicenti R K and Huq M S 1999 Changes in the size and location of kidneys from supine to standing positions and the implications for block placement during total body irradiation, *Int J Radiation Oncology Biol Phys* **45** No.2 447-449

Rosenstein M 1976 Organ doses in Diagnostic Radiology, US Department of Health, Education and Welfare, Bureau of Radiological Health, *BRH Tech Publ DA 76-8030*, Rockville Maryland 20857

Rosenstein M 1988 Handbook of Selected Tissue Doses for Projections Common in Diagnostic Radiology, US Department of Health, Education and Welfare, Bureau of Radiological Health, *BRH Tech Publ DA 89-8031*, Rockville Maryland 20857

Rubin R and Strayer D S 2008 Rubin's Pathology, 5th edition, page 848, Lippincott Williams & Wilkins and Wolters Kluwer Health, Baltimore, MD 21201, USA

Sato K, Noguchi H, Endo A, Emoto Y, Kogs S and Saito K 2007 Development of a voxel phantom of Japanese adult male in upright position, *Rad Prot Dos* **127** (1-4) 205-208

Sato K and Endo A 2008a Analysis of effects of posture on organ doses by internal photon emitters using voxel phantoms, *Phys Med Biol* **53** 4555-4572

Sato K, Endo A and Kimiaki S 2008b Dose Conversion Coefficients Using a Series of Adult Japanese Voxel Phantoms against External Photon Exposure, *Japan Atomic Energy Agency*, JAEA-DATA/Code 2008-016

Schultz F W Geleijns J and Zoetelief J 1994 Calculation of dose conversion factors for posterior-anterior chest radiography of adults with a relatively high-energy X-ray spectrum, *Br J Radiol*, **67** 775-785

Schultz F W Geleijns J and Zoetelief J 1995 Effetive Doses for different techniques used for PA chest radiography, *Rad Prot Dos* **57** Nos 1-4 371-376

Uustitupa T, Laakso I, Ilvonen S and Nikoskinen K 2010 SAR variation studyfrom 300 to 5000 MHz for 15 vocel models including different postures, *Phys Med Biol* **55** 1157-1176

Winslow M Huda W Xu X G Chao T C Shi C Y Ogden K M and Scalzetti M, 2004 Use of the VIP-Man Model to Calculate Energy Imparted and Effective Dose for X-Ray Examinations, *Health Physics* 86(2):174-182

Zankl M Panzer W and Herrmann C 2000 Calculation of Patient Doses Using a Human Voxel Phantom of Variable Diameter, *Rad Prot Dos* **90**, Nos 1-2 pp 155-158